The spatial extent of source influences on modeled column concentrations of short-lived species

A. J. Turner,[1] D. K. Henze,[1] R. V. Martin,[2,3] and A. Hakami[4]

[1] Providing top-down constraints on emissions is an important application of model-based analysis of remote-sensing observations of chemically reactive species, yet the degree to which column concentrations are governed by local vs distant sources within models themselves has yet to be fully characterized. We use a chemical transport model and its adjoint to quantify source contributions to weekly column concentrations of ammonia, nitrogen dioxide, sulfur dioxide, and formaldehyde. This efficient approach for quantifying the spatial extent of source influences is validated and then applied to an array of sites and seasons. Overall, we find instances for each species where emissions from at least 500 km away must be taken into account to retrieve 90% of the total column influence. This demonstrates that the common practice of assuming a local relationship between satellite observations and emissions in top-down constraints could lead to considerable biases, an issue that will be exacerbated as the resolution of models and observations are refined in coming years. **Citation:** Turner, A. J., D. K. Henze, R. V. Martin, and A. Hakami (2012), The spatial extent of source influences on modeled column concentrations of short-lived species, *Geophys. Res. Lett.*, *39*, L12806, doi:10.1029/2012GL051832.

1. Introduction

[2] Short-lived species (those with an atmospheric lifetime less than a few days) such as ammonia (NH_3), nitrogen oxides (NO_x), sulfur dioxide (SO_2), and formaldehyde (HCHO) play key roles in air quality and radiative forcing. NH_3 is the only base in sufficient quantities to neutralize a significant fraction of acids in the troposphere and as such has an important role in formation of ammonium sulfate and ammonium nitrate aerosol; NH_3 further leads to harmful levels of deposition of nitrogen into vegetation and ecosystems [*Rodhe et al.*, 2002; *Rabalais*, 2002]. NO_x is a criteria pollutant as well as a catalyst in the formation of tropospheric ozone, the latter which also impacts air quality and climate. SO_2 is the precursor of sulfate aerosol, which contributes to $PM_{2.5}$ and has numerous climate impacts. HCHO is produced by the oxidation of volatile organic compounds (VOCs) and can provide information about VOC emissions, which affect ozone and $PM_{2.5}$. Quantifying sources of these species is thus a concern for public health, climate change, and ecosystems. While direct in situ measurements provide valuable constraints on emissions, such data are generally quite sparse. Estimating emissions of these species and quantifying uncertainties in these estimates is an outstanding challenge.

[3] Satellite observations provide global measurements related to emissions; these observations can provide near-global measurements of vertical columns of several species relevant to air quality [*Fishman et al.*, 2008; *Martin*, 2008] and, as such, present new opportunities for constraining emissions. Numerous studies have performed top-down estimations of NO_x emissions [*Martin et al.*, 2003; *Jaeglé et al.*, 2004; *Konovalov et al.*, 2006; *Chai et al.*, 2009; *Lin et al.*, 2010]. HCHO columns have been used as a proxy for estimating VOC emissions [*Palmer et al.*, 2003; *Millet et al.*, 2008]. SO_2 emissions have been examined from top-down constraints [*Lee et al.*, 2011]. NH_3 is primarily emitted from livestock waste and fertilizers and concentrations can be estimated from remote-sensing observations [e.g., *Beer et al.*, 2008; *Clarisse et al.*, 2010; *Pinder et al.*, 2011].

[4] A common method of estimating emissions of short-lived species is to average a set of satellite measurements over a particular location and derive top-down constraints on surface emissions using a mass balance approach [e.g., *Martin et al.*, 2003; *Palmer et al.*, 2003; *Jaeglé et al.*, 2004; *Wang et al.*, 2007; *Zhao and Wang*, 2009; *Lin et al.*, 2010]. In this method, atmospheric transport is assumed to be negligible as the short chemical lifetime of the species translates to a smearing length scale less than the width of the model grid-cell [*Palmer et al.*, 2003]. Kernels have been used to account for the influence of adjacent cells [*Toenges-Schuller et al.*, 2006; *Boersma et al.*, 2008].

[5] Despite these previous studies, the degree to which column concentrations are governed by local vs distant sources within the models themselves has yet to be fully characterized. However, it is known that short-lived species impact the chemical state of the atmosphere beyond their own lifetime through reservoir species and chemical modes [e.g., *Prather*, 2007; *Goris and Elbern*, 2011]. Therefore, we focus on discerning local and nonlocal contributions to column concentrations in a global chemical transport model frequently employed for top-down constraints. Here we present and apply an approach to determine the spatial extent of source contributions to short-lived species (NH_3, NO_2, SO_2, and HCHO) using adjoint sensitivities.

2. Models

[6] GEOS-Chem is a global chemical transport model driven by assimilated meteorology from the Goddard Earth Observing System (GEOS-5) of the NASA Global Modeling

[1]Department of Mechanical Engineering, University of Colorado at Boulder, Boulder, Colorado, USA.
[2]Department of Physics and Atmospheric Science, Dalhousie University, Halifax, Nova Scotia, Canada.
[3]Harvard-Smithsonian Center for Astrophysics, Cambridge, Massachusetts, USA.
[4]Department of Civil and Environmental Engineering, Carleton University, Ottawa, Ontario, Canada.

Corresponding author: A. J. Turner, Department of Mechanical Engineering, University of Colorado at Boulder, 427 UCB, Boulder, CO 80309-0427, USA. (alexander.turner@colorado.edu)

and Assimilation Office (GMAO) [*Bey et al.*, 2001]. Here we use version 8.03.01 (www.geos-chem.org) with a horizontal resolution of $2° \times 2.5°$ and 47 vertical layers up to 0.01 hPa. GEOS-Chem accounts for both natural and anthropogenic emissions, gas phase chemistry, coupled oxidant-aerosol processes, carbonaceous aerosols, and sulfate-nitrate-ammonium aerosols [*Park et al.*, 2004]. NH_3 emissions are from the GEIA inventory and isoprene emissions are calculated using MEGAN [*Guenther et al.*, 2006]. Global NO_x and SO_x (SO_2 and primary sulfate are defined as one inventory in GEOS-Chem) emissions are from EDGAR [*Olivier et al.*, 2001], incorporated by *van Donkelaar et al.* [2008], overwritten with regional inventories for the US (NEI99), Europe (EMEP), southeast Asia [*Streets et al.*, 2006], and Mexico (BRAVO) [*Kuhns et al.*, 2003]. Biomass burning emissions are from *van der Werf et al.* [2006]. The GEOS-Chem adjoint [*Henze et al.*, 2007] solves a set of equations auxiliary to the forward model that efficiently calculate sensitivities of a scalar model response function with respect to numerous parameters.

3.   Sensitivity Metrics

[7] We derive equations for calculating the fraction of the spatial extent of emissions influencing a column concentration using adjoint sensitivities. We first define a response function to represent a model estimate of quantities typically used for top-down constraints. We consider a tropospheric column evaluated at a standard satellite overpass time (1:30 pm local time), averaged over a week,

$$\mathcal{J} = \frac{1}{n_t} \sum_{t=1}^{n_t} \left(\sum_{l=1}^{L} N \cdot C_{I,J,l,t} \right) \frac{1}{A_{I,J}}, \qquad (1)$$

where $C_{I,J,l,t}$ is species concentration (kg box^{-1}) at latitude I, longitude J, vertical layer l, and satellite overpass time t, n_t is the number of days, L is the index of the tropopause height, N is a factor for conversion from mass to molecules, and $A_{I,J}$ is column area (cm^2).

[8] We wish to calculate the partial derivative of $\mathcal{J}$ with respect to the emissions, $E_{i,j,k}$, from emission sector k,

$$\lambda_{i,j,k} = \frac{\partial \mathcal{J}}{\partial E_{i,j,k}} E_{i,j,k}, \qquad (2)$$

where $\lambda_{i,j,k}$ is the adjoint sensitivity with respect to a single species emission from sector k at latitude i, longitude j, and $E_{i,j,k}$ is the total emission in column i, j of this species from sector k. The adjoint sensitivity, λ, is thus the sensitivity with respect to fractional emissions changes, the units of which are consistent with those of $\mathcal{J}$. The sum of all λ would represent a first order approximation of the column, $\mathcal{J}$. The advantage of calculating these sensitivities using the adjoint model is that the influence from all model grid cells, species and sectors, can be obtained in a single adjoint model evaluation. In contrast, such sensitivities would require numerous model evaluations using traditional sensitivity techniques.

[9] We can define a cumulative sensitivity metric for each species as the fraction of the sensitivity of a column density to emissions that comes from emissions within a radial distance d of the column center at I, J,

$$F_K^d = \frac{\sum\limits_{i \in d} \sum\limits_{j \in d} \sum\limits_{k \in K} |\lambda_{i,j,k}|}{\sum\limits_{i} \sum\limits_{j} \sum\limits_{k \in K} |\lambda_{i,j,k}|}, \qquad (3)$$

where K is the set of all emissions sectors for a single species (e.g., anthropogenic, natural, and biomass NH_3). We note the distance d is based on grid box centers and is thus approximate to within a grid-box width which itself may be a few hundred kilometers wide. Both the numerator and denominator in equation (3) are defined using absolute values as we are interested in total sensitivities, not just positive or negative influences. Additionally, the cases examined in this study have negligible negative sensitivities (generally <1% of the positive sensitivities). The fraction accounted for in the mass balance approach would be the contribution from only emissions of species K local to the column (i.e., considering only $i, j = I, J$ in the numerator of equation (3)).

4.   Validation

[10] Here we validate the accuracy of the adjoint sensitivities and assess the extent to which they can be used for source attribution. For the former goal, we can approximate the adjoint sensitivities ($\lambda_{i,j,k}$, which should be the partial derivative of $\mathcal{J}$ with respect to the emission scaling factors, ξ) with finite difference sensitivities computed using consecutive forward model evaluations,

$$\lambda_{k,i,j} \approx \frac{\mathcal{J}(\xi + \delta\xi) - \mathcal{J}(\xi - \delta\xi)}{2\delta\xi}, \qquad (4)$$

where $\delta\xi$ is a small perturbation in the emission scaling factor. However, a limitation is that the finite difference method can only be used to estimate the sensitivity to one emission sector at a time. As such, we only validate the sensitivity of one emission sector for each species due to the computational expense of the finite difference calculations. A comparison of NH_3, NO_x, SO_2, and HCHO sensitivities using finite difference methods (equation (4)) with the adjoint method (equation (2)) can be seen in Figures 1a–1d. A visual inspection of these shows the methods are in agreement with the exception of NO_x at the Ocean site. For this site we performed another test with a smaller perturbation of $\delta\xi = 0.05$, which is plotted as a square, and can be seen in Figure 1b falling on unity. Additional validation can be seen in the ratio of adjoint to finite difference sensitivities in Figure S3 in the auxiliary material.[1] Overall, the adjoint and finite difference sensitivities are consistently in agreement.

[11] Having validated that the adjoint model gives correct gradients, it is important to assess over what range these can be used to approximate total source contributions, as use of adjoint sensitivities for source attribution assumes a linear source–receptor relationship. We perform "zero-out" tests, see Figures 1e–1h, from the difference of two forward model runs, one with a 100% reduction to emissions in the test location. NH_3, SO_2, and HCHO still show a consistently linear trend about unity. NO_x shows a larger scatter about unity indicating a less linear source–receptor relationship, particularly in the Europe test site (see Figures 1f and S3f). This is expected owing to nonlinearities of NO_x photochemistry. While the nonlinear response of NO_2 to perturbations of NO_x emissions in a single grid cell at a time is found to be small for 10% perturbations and within a factor
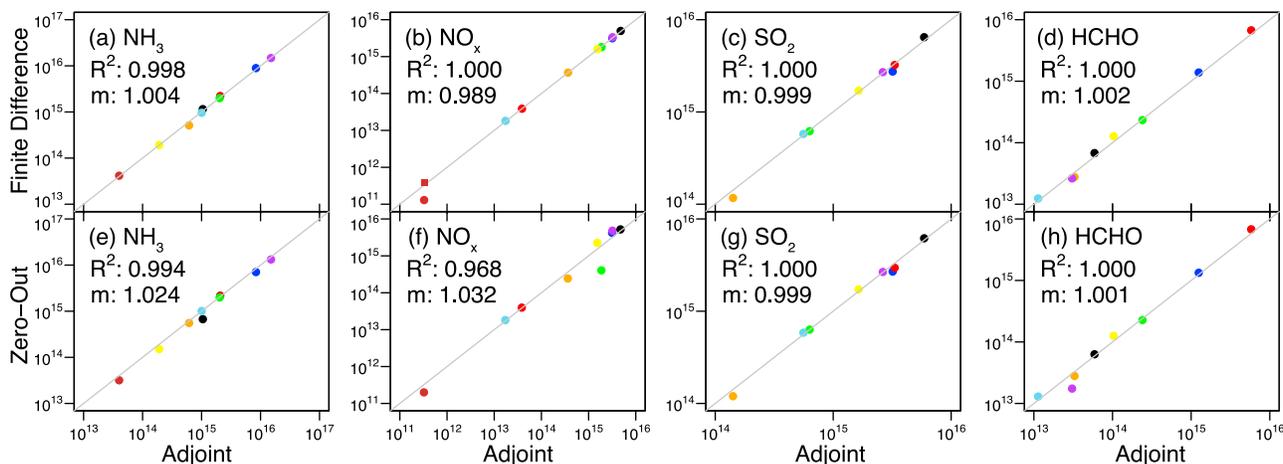

Figure 1. Comparison of adjoint and finite difference sensitivities for Africa (orange), America (red), Australia (yellow), China (blue), Europe (green), India (purple), Ocean (brown), SAfrica (black), and SAmerica (cyan). (a–d) Comparison of adjoint sensitivities (equation (2)) with finite difference sensitivities (equation (4)) with $\delta\xi = 0.1$; the brown square in Figure 1b is the Ocean site using a perturbation of $\delta\xi = 0.05$. (e–f) "Zero-out" tests with a 100% reduction in emissions. All units are molec cm^{-2}.

of two for 100% perturbations in most of the sites modeled here, such behavior could vary substantially depending upon the type of source and model resolution [*Valin et al.*, 2011].

[12] Nonlinearity in atmospheric responses occur when the perturbation of an input, such as emissions, is large enough to shift the chemical state of the atmosphere to a regime that has a sufficiently different response surface. For example, previous works on forward sensitivity analysis [*Hakami et al.*, 2004; *Cohan et al.*, 2005] have suggested a range of 30%–50% over which linear sensitivities would be reasonably accurate for ozone. Forward sensitivity studies often employ domain-wide perturbations to emissions while adjoint studies focus on individual source impacts. Changes in emissions from individual sources are less likely to trigger significant shifts in the chemical regime. Therefore, contributions from individual sources are expected to exhibit a close to linear response over a wider range than those typically reported for forward sensitivities.

5. Results and Discussion

[13] The cumulative sensitivity fractions, F_K^d, are estimated for four chemical species: NH$_3$, NO$_2$, SO$_2$, and HCHO. The simulations are three-weeks in duration, and the response function is evaluated once daily during the final week at the satellite overpass time. The sites used in the simulation and the relevant emissions can be seen in Figures S1 and S2. The China, America, and Europe sites are used for sensitivity analysis while the other sites are used only for validation. The China, America, and Europe sites were selected based on geographic and environmental differences. Namely, the China site was selected for the large spatial variability in emissions, large magnitude of emissions, and an overall polluted environment. The Europe site was selected for its relatively low and spatially homogeneous emissions. The America site was selected for its high isoprene emissions and moderate emissions of NH$_3$, NO$_x$, and SO$_2$. Additionally, the sites were selected for their varying latitudes in the northern hemisphere (31°N–52°N). To address the seasonality of the results we perform our analysis during July

(1st–22nd) and December (1st–22nd) of 2005. To address spatial variability, we examine four cells neighboring our designated sites $[(I+1, J), (I-1, J), (I, J+1),$ and $(I, J-1)]$. For this study we considered the set of emitted species, K: anthropogenic, biofuel, and biomass burning (NH$_3$, NO$_x$, SO$_2$, and isoprene) as well as natural NH$_3$, soil NO$_x$, lightning NO$_x$, aircraft NO$_x$, and ship SO$_2$. The results in Figure 2 show the cumulative sensitivity fraction as a function of radial distance from the column (dark line), with the variability from repeated tests in four adjacent cells indicated by shading; more of the column influence is recovered as we sum across larger distances. Additionally, the dashed line with a triangle (circle) at the base indicates the radial distance necessary to account for 63% (90%) of the total emission influence, and this distance will hereafter be referred to as d_{63} (d_{90}). Table S1 lists d_{63} and d_{90} for all cases.

[14] For this set of cases, we first apply equation (3) to tropospheric NH$_3$. From Figure 2a we can see Europe has the largest d_{90} and lowest local influence with only 19.5% of the NH$_3$ column owing to local emissions of NH$_3$ indicating that up to 80.5% of the NH$_3$ column in I, J is governed by emissions of NH$_3$ outside this cell. Additionally, Europe has the smallest spatial variance in both July and December; this small spatial variance is likely owing to this site having the most uniform emissions distributions of the three test sites. Similarly, the largest spatial variance is in China owing to the large emissions variance. NH$_3$ exhibits large seasonal variability in China and America (Figures 2a and 2b), with the local contribution decreasing from July to December and d_{90} increasing from July to December. Overall, for NH$_3$ we found that the modeled local contribution ranges from 13.4%–70.0% in summer and 10.2%–42.3% in winter.

[15] Next considering NO$_2$, the China test site exhibits the largest local contribution during July (Figure 2c) but again has the largest spatial variability owing to the emissions variance. All sites show substantial seasonal variability (~20%) and a slight increase in d_{90} with the largest seasonal effects occurring at the northernmost latitude (Europe), because the NO$_x$ lifetime is largely determined by photochemistry. Overall, for NO$_2$ we found that the local
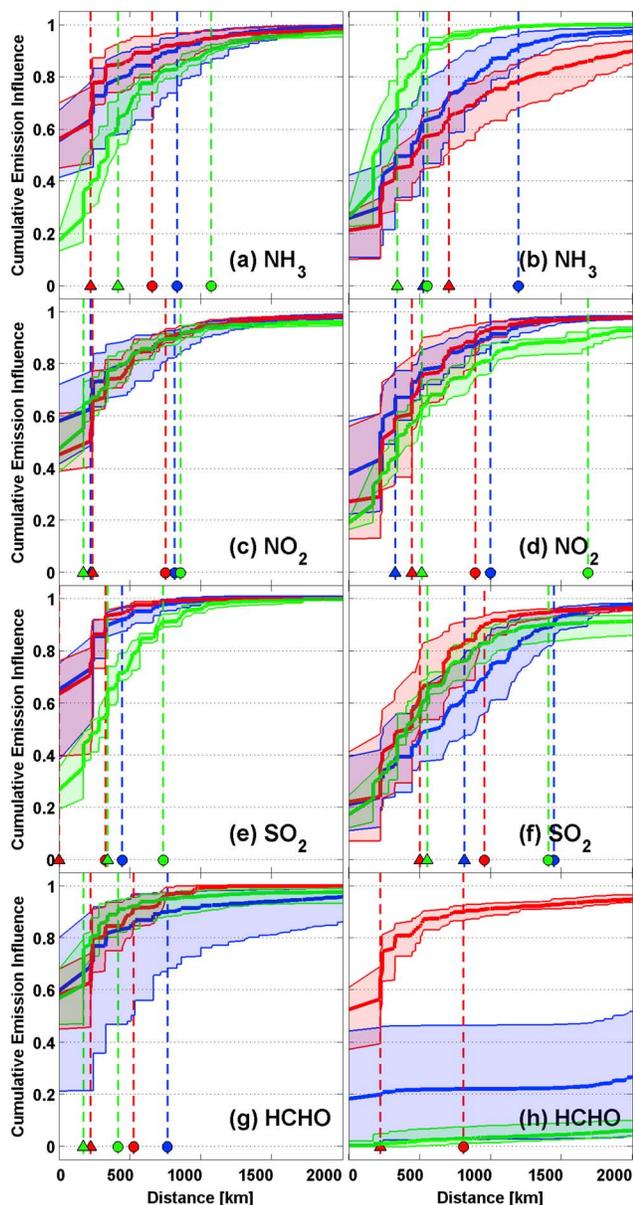
Figure 2. Cumulative emission influence as a function of distance for the China (blue), America (red), and Europe (green) test sites. Simulations from (a, c, e, g) July and (b, d, f, h) December 2005. The dark lines indicate the average of simulations at (I, J), $(I + 1, J)$, $(I - 1, J)$, $(I, J + 1)$, and $(I, J - 1)$ while the shaded region is the maximum and minimum of these. The vertical dashed lines with triangles (circles) at the base indicate the distance, d_{63} (d_{90}), from the test location over which the mean F_K^d must be summed in order to account for 63% (90%) of the total emission influence.

contribution ranges from 38.6%–72.0% in summer and 13.1%–58.0% in winter.

[16] For SO_2, we again see the lowest local contribution in the winter at the Europe test site in Figure 2f. SO_2 lifetime is primarily dictated by photochemistry and aqueous chemistry. This aqueous chemistry has a strong seasonal dependence at the China test site likely driven by monsoons and seasonal rainfall in this region. July is in the monsoon season for China while December is in the dry season. Overall, for

SO_2 we found the modeled local contribution ranges from 19.4%–76.0% in summer and 7.3%–41.3% in winter.

[17] For HCHO, examination of Figures 2g and 2h yields a strong seasonal dependence at all test sites indicated by an increased d_{90} of 1635 km, 282 km, and 9330 km at the China, America, and Europe sites respectively. HCHO is treated here as a proxy only for isoprene emissions. Consideration of other VOC sources could reduce d_{90} and its seasonal variability. Additionally, we see large spatial variability at the China site due in part to the heterogeneous emissions in the region (see Figures S1 and S2). Overall, for HCHO we found the modeled local contribution ranges from 21.4%–80.0% in summer and 0.1%–61.0% in winter.

[18] The use of a smearing length scale in mass-balance inversions corresponds to an assumption that 63% of the emissions influence comes from within the column. Overall, we see this criterion is satisfied for SO_2 at the America and China sites in July. The results suggest that accounting for transport from at least one grid cell away is necessary to reach this criteria in July for NH_3, NO_2, and HCHO at each site and SO_2 in Europe. Lastly, we note that most (17 of 18) cases in Figure 2 show an increase in the spatial region required to return 90% of the total column influence, d_{90}, from July to December as the winter will generally have less active photochemistry leading to increasing chemical lifetimes and longer transport timescales. Additional tests indicate that the nonlocal influences on monthly average column concentrations are within the same range as those for the mean across multiple weekly average columns (see Figure S4).

6. Conclusions

[19] Here we demonstrate that nonlocal sources contribute substantially to average tropospheric column estimates of short-lived species. Mechanistically, such influences are not necessarily owing to transport alone; short-lived species can have long-range impacts through reservoir species and chemical feedbacks. NO_x emissions can have long-range impacts through peroxyacetyl nitrate and chemical feedbacks with ozone; nonlocal contributions of NH_3 can result from aerosol thermodynamics while nonlocal contributions of isoprene can result from chemical cycling. The consequence of such feedbacks is that emissions outside the base of a column at coarse resolution ($\sim 2°$) may govern more than 50% of the model's column concentration and to retrieve 90% of the total column influence may require accounting for emissions from more than 500 km away. At this resolution, inventories in Europe have relatively uniform emissions of NH_3, NO_x, SO_2, and isoprene, leading to consistently small local contributions and small spatial variability. Conversely, test sites in China in general have the largest spatial variance in emissions, resulting in the largest spatial variance in contributions. While this is not an exhaustive study, nor a rigorous case-by-case assessment of the conditions leading to these nonlocal influences, the potential for large nonlocal contributions demonstrated here motivates additional attention to spatial attribution errors in the mass balance approach for top-down constraints. The results presented here provide a framework for assessing the importance of such effects for top-down constraints which may guide method selection or kernel implementation in future studies. Quantifying these errors is thus warranted for further assessment.

References

Beer, R., et al. (2008), First satellite observations of lower tropospheric ammonia and methanol, *Geophys. Res. Lett.*, *35*, L09801, doi:10.1029/2008GL033642.

Bey, I., D. J. Jacob, R. M. Yantosca, J. A. Logan, B. D. Field, A. M. Fiore, Q. Li, H. Y. Liu, L. J. Mickley, and M. G. Schultz (2001), Global modeling of tropospheric chemistry with assimilated meteorology: Model description and evaluation, *J. Geophys. Res.*, *106*(D19), 23,073–23,095, doi:10.1029/2001JD000807.

Boersma, K. F., et al. (2008), Validation of OMI tropospheric NO_2 observations during INTEX-B and application to constrain NO_x emissions over the eastern United States and Mexico, *Atmos. Environ.*, *42*, 4480–4497.

Chai, T., G. R. Carmichael, Y. Tang, A. Sandu, A. Heckel, A. Richter, and J. P. Burrows (2009), Regional NO_x emission inversion through a four-dimensional variational approach using SCIAMACHY tropospheric NO_2 column observations, *Atmos. Environ.*, *43*, 5046–5055.

Clarisse, L., C. Clerbaux, F. Dentener, D. Hurtmans, and P. F. Coheur (2010), Global ammonia distribution derived from infared satellite observations, *Nat. Geosci.*, *2*, 479–483, doi:10.1038/ngeo551.

Cohan, D. S., A. Hakami, Y. Hu, and A. G. Russell (2005), Nonlinear response of ozone emissions: Source apportionment and sensitivity analysis, *Environ. Sci. Technol.*, *39*(17), 6739–6748.

Fishman, J., et al. (2008), Remote sensing of tropospheric pollution from space, *Bull. Am. Meteorol. Soc.*, *89*(6), 805–821.

Goris, N., and H. Elbern (2011), Singular vector decomposition for sensitivity analyses of tropospheric chemical scenarios, *Atmos. Chem. Phys. Discuss.*, *11*, 16,745–16,799, doi:10.5194/acpd-11-16745-2011.

Guenther, A., T. Karl, P. Harley, C. Wiedinmyer, P. I. Palmer, and C. Geron (2006), Estimates of global terrestrial isoprene emissions using MEAGAN (Model of Emissions of Gases and Aerosols from Nature), *Atmos. Chem. Phys.*, *6*, 3181–3210.

Hakami, A., M. T. Odman, and A. G. Russell (2004), Nonlinearity in atmospheric response: A direct sensitivity analysis approach, *J. Geophys. Res.*, *109*, D15303, doi:10.1029/2003JD004502.

Henze, D. K., A. Hakami, and J. H. Seinfeld (2007), Development of the adjoint of GEOS-Chem, *Atmos. Chem. Phys.*, *7*, 2413–2433.

Jaeglé, L., R. V. Martin, K. Chance, L. Steinberger, T. P. Kurosu, D. J. Jacob, A. I. Modi, V. Yoboué, L. Sigha-Nkamdjou, and C. Galy-Lacaux (2004), Satellite mapping of rain-induced nitric oxide emissions from soils, *J. Geophys. Res.*, *109*, D21310, doi:10.1029/2004JD004787.

Konovalov, I. B., M. Beekmann, A. Richter, and J. P. Burrows (2006), Inverse modeling of the spatial distribution of NO_x emissions on a continental scale using satellite data, *Atmos. Chem. Phys.*, *6*, 1747–1770.

Kuhns, H., M. Green, and V. Etyemezian (2003), Big Bend Regional Aerosol and Visibility Observational (BRAVO) study emissions inventory, report prepared for BRAVO Committee, technical report, Desert Res. Inst., Las Vegas, Nev.

Lee, C., R. V. Martin, A. van Donkelaar, H. Lee, R. R. Dickerson, J. C. Hains, N. Krotkov, A. Richter, K. Vinnikov, and J. J. Schwab (2011), SO_2 emissions and lifetimes: Estimates from inverse modeling using in situ and global, space-based (SCIAMACHY and OMI) observations, *J. Geophys. Res.*, *116*, D06304, doi:10.1029/2010JD014758.

Lin, J. T., M. B. McElroy, and K. F. Boersma (2010), Constraint of anthropogenic NO_x emissions in China from different sectors: A new methodology using multiple satellite retrievals, *Atmos. Chem. Phys.*, *10*, 63–78, doi:10.5194/acp-10-63-2010.

Martin, R. (2008), Satellite remote sensing of surface air quality, *Atmos. Environ.*, *42*, 7823–7843.

Martin, R. V., D. J. Jacob, K. Chance, T. P. Kurosu, P. I. Palmer, and M. J. Evans (2003), Global inventory of nitrogen oxide emissions constrained by space-based observations of NO_2 columns, *J. Geophys. Res.*, *108*(D17), 4537, doi:10.1029/2003JD003453.

Millet, D. B., D. J. Jacob, K. F. Boersma, T.-M. Fu, T. P. Kurosu, K. Chance, C. L. Heald, and A. Guenther (2008), Spatial distribution of isoprene emissions from North America derived from formaldehyde column measurements by the OMI satellite sensor, *J. Geophys. Res.*, *113*, D02307, doi:10.1029/2007JD008950.

Olivier, J. G. J., J. J. M. Berdowski, J. A. H. W. Peters, J. Bakker, A. J. H. Visschedijk, and J. P. J. Bloos (2001), Applications of EDGAR including a description of EDGAR 3.2: Reference database with trend data for 1970–1995, *RIVM Rep. 773301 001*, Natl. Inst. for Public Health and the Environ., Bilthoven, Netherlands.

Palmer, P. I., D. J. Jacob, A. M. Fiore, R. V. Martin, K. Chance, and T. P. Kurosu (2003), Mapping isoprene emissions over North America using formaldehyde column observations from space, *J. Geophys. Res.*, *108*(D6), 4180, doi:10.1029/2002JD002153.

Park, R. J., D. J. Jacob, B. D. Field, R. M. Yantosca, and M. Chin (2004), Natural and transboundary pollution influences on sulfate-nitrate-ammonium aerosols in the United States: Implications for policy, *J. Geophys. Res.*, *109*, D15204, doi:10.1029/2003JD004473.

Pinder, R. W., J. T. Walker, J. O. Bash, K. E. Cady-Pereira, D. K. Henze, M. Luo, G. B. Osterman, and M. W. Shephard (2011), Quantifying spatial and seasonal variability in atmospheric ammonia with in situ and space-based observations, *Geophys. Res. Lett.*, *38*, L04802, doi:10.1029/2010GL046146.

Prather, M. J. (2007), Lifetimes and time scales in atmospheric chemistry, *Philos. Trans. R. Soc. A*, *365*, 1705–1726, doi:10.1098/rsta.2007.2040.

Rabalais, N. N. (2002), Nitrogen in aquatic ecosystems, *Ambio*, *31*(2), 102–112.

Rodhe, H., F. Dentener, and M. Schulz (2002), The global distribution of acidifying wet deposition, *Environ. Sci. Technol.*, *36*(20), 4382–4388.

Streets, D. G., Q. Zhang, L. Wang, K. He, J. Hao, Y. Wu, Y. Tang, and G. R. Carmichael (2006), Revisiting China's CO emissions after the Transport and Chemical Evolution over the Pacific (TRACE-P) mission: Synthesis of inventories, atmospheric modeling, and observations, *J. Geophys. Res.*, *111*, D14306, doi:10.1029/2006JD007118.

Toenges-Schuller, N., O. Stein, F. Rohrer, A. Wahner, A. Richter, J. P. Burrows, S. Beirle, T. Wagner, U. Platt, and C. D. Elvidge (2006), Global distribution pattern of anthropogenic nitrogen oxide emissions: Correlation analysis of satellite measurements and model calculations, *J. Geophys. Res.*, *111*, D05312, doi:10.1029/2005JD006068.

Valin, L. C., A. R. Russell, R. C. Hudman, R. C. Cohen. (2011), Effects of model resolution on the interpretation of NO_2 observations, *Atmos. Chem. Phys.*, *11*, 11,647–11,655.

van der Werf, G. R., J. T. Randerson, L. Giglio, G. Collatz, P. Kasibhatla, and A. F. Arellano Jr (2006), Interannual variability in global biomass burning emissions from 1997 to 2004, *Atmos. Chem. Phys.*, *6*, 3423–3441.

van Donkelaar, A., et al. (2008), Analysis of aircraft and satellite measurements from the Intercontinental Chemical Transport Experiment (INTEX-B) to quantify long-range transport of East Asian sulfur to Canada, *Atmos. Chem. Phys.*, *8*, 2999–3014.

Wang, Y., M. B. McElroy, R. V. Martin, D. G. Streets, Q. Zhang, and T.-M. Fu (2007), Seasonal variability of NO_x emissions over east China constrained by satellite observations: Implications for combustion and microbial sources, *J. Geophys. Res.*, *112*, D06301, doi:10.1029/2006JD007538.

Zhao, C., and Y. Wang (2009), Assimilated inversion of NO_x emissions over east Asia using OMI NO_2 column measurements, *Geophys. Res. Lett.*, *36*, L06805, doi:10.1029/2008GL037123.